Local Flame Structure of Turbulent Premixed Flames -DNS and CH/OH PLIF-

Mamoru TANAHASHI, Yuzuru NADA, Shunsuke TSUKINARI, Toshihiko SAITOH, Toshio MIYAUCHI
Department of Mechanical and Aerospace Engineering, Tokyo Institute of Technology,
2-12-1 Ookayama, Meguro-ku, Tokyo 152-8552, Japan

Gyung-Min CHOI
National Aerospace Laboratory,
7-44-1 Jindaiji-Higashi, Chofu, Tokyo 182-8522, Japan

In this study, three-dimensional direct numerical simulation (DNS) of H_2-air premixed flames has been performed to clarify local flame structure in turbulent premixed flames. The heat release rate tends to increase at the flame convex toward burned side regardless of turbulent characteristics. Three-dimensional handgrip structure generated by fine scale eddy leads to increase heat release rate compared with that of laminar flame. Two-dimensional DNS of CH_4-air turbulent premixed flames are also conducted to investigate the local flame structure as well as the relation between heat release rate and species mole fraction. A pocket is observed in both unburned and burned side, which is consistent with the result of three-dimensional DNS. The distribution of heat release rate agrees with that of CH mole fraction even in high intensity turbulent premixed flames. Finally, the local flame structure and pressure fluctuations in the oscillating turbulent premixed flame are investigated by CH/OH PLIF and pressure measurement. The degree of wrinkling changed in terms of Reynolds number and equivalence ratio, and the local flame structure became more complicated with increasing Reynolds number. The observed scale of weak wrinkled flame front and flame cusps corresponds to integral length scale and Taylor micro scale of unburned mixture, respectively. The local flame structure is influenced by pressure fluctuations in the oscillation turbulent flames, and a relation between local flame structure and long period of pressure fluctuation is observed.

1. Introduction

In the development of high efficiency combustor, it is important to inhibit the combustion-driven oscillations or combustion instabilities. Combustion-driven oscillations may cause undesirable results, such as mechanical vibration and destruction of system, etc. Among them, self-excited oscillations caused by the resonance between the pressure fluctuations and heat release rate in a combustion chamber (Putnum 1971). Recently, active feedback controls of the combustor have been reported by many researchers (Paschereit *et al.* 1999, Lee *et al.* 2000, Harper *et al.* 2001). The active controls have possibilities to develop quite high efficiency and stable combustors. To develop the active control scheme of the combustors, the understandings of the flame structures in the combustor are necessary. Especially, detailed information about heat release rate or pressure fluctuations in the turbulent flames is quite important for development of active control scheme.

The local flame structure in turbulence has been considered to depend on the ratios of turbulence intensity to laminar burning velocity (u'/S_L) and integral length scale to laminar flame thickness (l/d_F) (Peters 2000). From these ratios, the local flame structure has been classified into wrinkled flamelets, corrugated flamelets, thin reaction zones and broken reaction zones. In DNS, all of the information concerning the flame structure can be obtained and systematic selection of u'/S_L and l/d_F is relatively easy compared with the experiments. Baum *et al.* (1994) have conducted DNS of two dimensional H_2/air turbulent premixed flames with detailed kinetics mechanism and showed the effect of turbulent characteristics on local flame structure. Tanahashi *et al.* (2001) have conducted two-dimensional DNS of H_2/air turbulent premixed flames to clarify the effect of turbulence intensity on the local flame structure. They have showed that the flame in turbulence becomes very complicated with the increase of turbulence intensity and corrugated flames and pocket structure of unburned mixture are observed.

Recently, due to remarkable development of computer technology, three-dimensional DNS become possible. DNS of turbulence has been conducted to clarify the structure of small-scale motion in turbulence. Tanahashi *et al.* (1997) have showed that homogeneous isotropic turbulence consists of a lot of similar tube-like eddies which show swirling motions. These tube-like eddies are called as 'coherent fine scale eddy'. Coherent fine scale eddy is universal structure of turbulence, and mean diameter of this eddy is about 8 times of Kolmogorov micro scale and maximum of the mean azimuth velocity is about 0.6 times of the root mean square of velocity fluctuation. The coherent fine scale eddy influences local flame

structure of turbulent flames. DNS of premixed flames in homogeneous isotropic turbulence has been conducted to investigate the interaction between flame and coherent fine scale eddy and it is clarified that the local flame structure depends on the angle between flame front and axis of coherent fine scale eddy (Tanahashi *et al*. 2000). Tanahashi *et al*. (2000, 2002) clarified the local flame structure in corrugated flamelets and thin reaction zones. However, it is necessary that we take more informations about local flame structure in various combustion regimes.

For practical active control of combustion-driven oscillation, detailed information about local flame structure in the oscillating turbulent flames is necessary. Because it is very hard to investigate the practical combustion-driven oscillations by DNS, experimental approaches are also demanded to establish effective active control scheme. Due to remarkable developments of the laser diagnostics of the combustion field, detailed structure of the turbulent flames can be measured by a particle image velocimetry (PIV), a planar laser-induced fluorescence (PLIF) etc. Especially, CH PLIF measurements have been used to investigate the flame fronts in turbulence because CH radicals are produced at the flame front and have very narrow width enough to represent the reaction zone (Allen *et al.* 1986, Monsour *et al.* 1998, Carter *et al.* 1998). Furthermore, it is well known that distribution of CH radicals agrees with that of the heat release rate. Since the heat release rate plays important roles in the sound generation mechanism in turbulence combustion field, CH PLIF measurement may provide the information about spatial and temporal fluctuations of the heat release rate. By understandings spatial and temporal fluctuations of the heat release rate in the combustor, the development of the active controls scheme becomes easier because the dominant sound source can be identified in the developing process. However, because CH PLIF indicates primary reaction zone, it is hard to understand the local flame structure in the turbulent flame from single measurement of CH PLIF. The simultaneous measurement of CH and OH, therefore, may promise better information of the instantaneous local flame structure in the oscillating turbulent flames.

In present study, we have conducted three-dimensional DNS of H_2-air turbulent premixed flames and two-dimensional DNS of CH_4-air turbulent premixed flames in section 2. For H_2-air turbulent premixed flames, the relation between three-dimensional structure and heat release rate is investigated. For CH_4-air turbulent premixed flames, heat release rate and species distribution such as CH and OH is investigated. In section 3, the simultaneous CH and OH fluorescence measurements have been conducted for CH_4-air turbulent premixed flames on swirl burner. The effect of equivalence ratio on local flame structure and the relation between fluctuation of pressure and local flame structure is investigated.

2. Direct numerical simulation of turbulent premixed flames

2.1 Numerical Methods

In this study, the external forces, Soret effect, Dufour effect, pressure gradient diffusion, bulk viscosity and radiative heat transfer are assumed to be negligible. In this study, DNS of H_2-air turbulent premixed flames and CH_4-air turbulent premixed flames are conducted with detailed kinetic mechanism. For H_2-air turbulent premixed flames, the three-dimensional DNS code developed in our previous study (Miyauchi *et al*. 1996) was used, and the detailed kinetic mechanism (Gutheil *et al*. 1993) which includes 27 elementary reactions and 12 reactive species (H_2, O_2, H_2O, O, H, OH, HO_2, H_2O_2, N_2, N, NO_2 and NO) was taken to represent hydrogen/air reaction in turbulence. For CH_4-air turbulent premixed flames, the two-dimensional DNS code (MKTFS) (Tanahashi *et al.* 2000), which can simulate any detailed kinetic mechanisms, was used, and GRI Mech. 2.11 which includes 279 elementary reactions and 48 reactive species are used to represent methene/air reaction in turbulence. The temperature dependence of the viscosity, the thermal conductivity and the diffusion coefficients are considered by linking CHEMKIN packages (Kee *et al*. 1986, 1989) with modifications to vector/parallel computation. Diffusion coefficients of each species are given as those for the mixture calculated from the ordinary binary diffusion coefficients at each gird point. The governing equations are discretized by 4th-order central difference scheme in the x direction, and by a Fourier spectral method in the other directions. Figure 1 shows the schematic of the flow field used in H_2-air turbulent premixed flames. The boundary conditions in the x direction are NSCBC (Poinsot *et al*. 1992, Baum *et al*. 1994) and those in the y and z directions are periodic. Time integration is implemented by the third-order Runge-Kutta scheme. For CH_4-air turbulent premixed flames, The boundary conditions in the x and y direction are NSCBC and periodic, respectively. Time integration is Adams-Bashforce scheme.

Numerical parameters of DNS conducted in the present study are listed in Table 1. Calculations are conducted for representative three and five cases of H_2-air and CH_4-air turbulent premixed flames that have different u'_{rms}/S_L and l/d_F. H_2-air and CH_4-air mixture are set to f =1.0 at 0.1MPa and 700K for all cases. In this study, the inflow boundary condition for the velocity field was given as $u_{in}=S_L+u'$. The turbulence u' was obtained through the preliminary DNS of homogeneous isotropic turbulence by a spectral method. For H_2-air turbulent premixed flames, the initial condition of this preliminary DNS was given by the energy

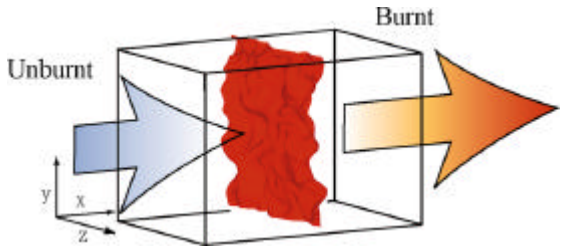

Fig. 1 Geometry of flow field used in DNS of turbulent premixed flames.

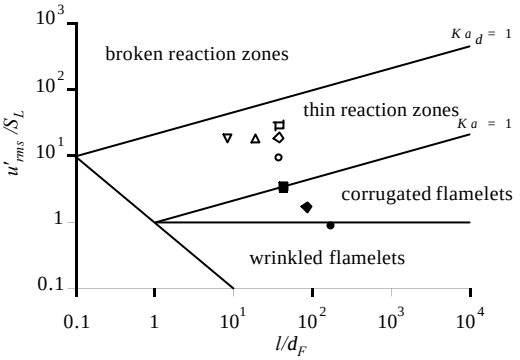

Fig. 2 Numerical conditions of DNS in turbulent combustion diagram.

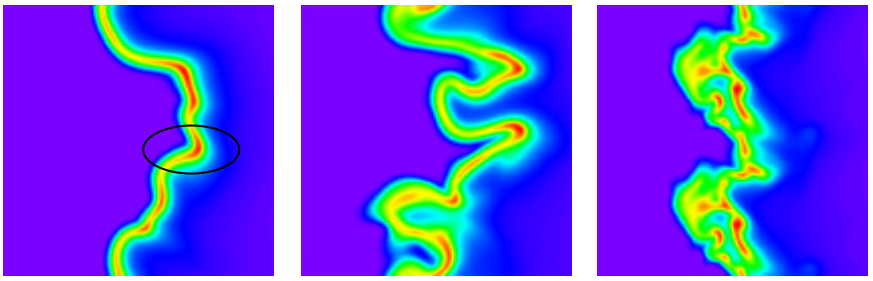

(a) H_2-Case 1 (b) H_2-Case 2 (c) H_2-Case 3

Fig. 3 Distributions of the heat release rate on a typical *x-z* plane.

Table 1 Numerical parameters for DNS of turbulent premixed flames.

	Re_l	Re_l	l/d_F	u'_{rms}/S_L	D/d_l	l/d_l	$L_x \times L_y \times L_z$ (mm)	$N_x \times N_y \times N_z$
H_2-Case 1	143.6	37.4	168.6	0.85	0.78	3.38	5×10×10	257×256×256
H_2-Case 2	143.6	37.4	84.3	1.70	0.39	1.69	10×5×5	513×128×128
H_2-Case 3	143.6	37.4	42.2	3.41	0.19	0.85	5×2.5×2.5	513×128×128
CH_4-Case 1	350.5	116.4	37.9	9.24	-	5.03	10.5×10.5	1281×768
CH_4-Case 2	705.1	224.7	37.3	18.89	-	4.95	10.5×10.5	1281×768
CH_4-Case 3	1073.7	334.4	37.1	28.92	-	4.93	10.5×10.5	1281×768
CH_4-Case 4	350.5	116.3	19.0	18.5	-	2.52	10.5×5.25	1281×512
CH_4-Case 5	148.3	51.59	8.1	18.2	-	1.08	5.4×2.16	1281×512

spectrum that has been reported by Comte-Bellot and Corrsin (1971) in the grid turbulence. The same homogeneous isotropic turbulence is used for H_2-air turbulent premixed flames in the non-dimensional space, therefore the product of u'_{rms}/S_L and l/d_F are constant. In our previous study using three-dimensional DNS of H_2-air turbulent premixed flames (Tanahashi *et al*. 2000), it has been shown that the coherent fine scale eddy in turbulence plays important roles on the local flame structure of the turbulent premixed flames. In Table 1, the ratios of the most expected diameter of the coherent fine scale eddy to the laminar flame thickness are presented. Note that the most expected diameter is about 8 times the Kolmogorov micro scale.

In Figure 2, locations of each case are plotted in the turbulent combustion diagram proposed by Peters (2000). For H_2-air turbulent premixed flames, H_2-Case 1 to H_2-Case 3 are classified in wrinkled flamelets, corrugated flamelets and thin reaction zones near the boundary of Ka=1.0, respectively. For CH_4-air turbulence premixed flames, all cases are classified in thin reaction zones.

2.2 Local flame structure obtained by DNS

The distributions of heat release rate on a typical *x-z* plane obtained by three-dimensional DNS for H_2-air turbulent premixed flames are shown in Fig. 3. The size of region in Fig. 3 is 5 mm × 5 mm. In H_2-Case 1, the heat release rate is fluctuating and the flame convex toward burned side shows high heat release rate compared with that of laminar flame as shown by the circle in Fig. 2 (a). In our previous study (Tanahashi *et al*. 2000), it is clarified that fine scale eddy parallel to flame front transports unburned gas into the flame by strong swirling motion and generates the region of high heat release rate. These results indicate that local flame structure in wrinkled flamelets is modified by the turbulence motion. The fluctuation of heat release rate in H_2-Case 2 and H_2-Case 3 is very large as shown in Fig. 2 (b) and (c).

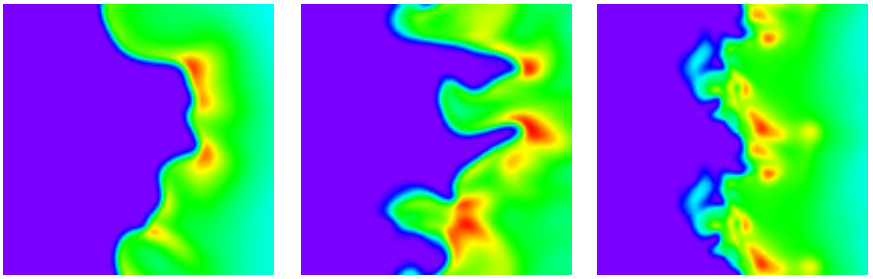

(a) H_2-Case 1 (b) H_2-Case 2 (c) H_2-Case 3

Fig. 4 Distributions of the mass fraction of O atom on a typical *x*-*z* plane.

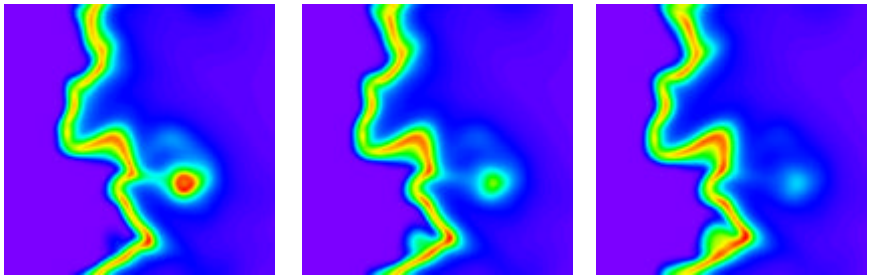

Fig. 5 Distributions of heat release rate in H_2-Case 2 at three different times (time interval = $0.1t_l$).

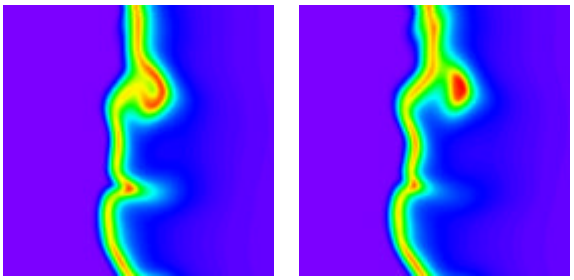

Fig. 6 Distributions of heat release rate in H_2-Case 1 at two different times (time interval =$0.04t_l$).

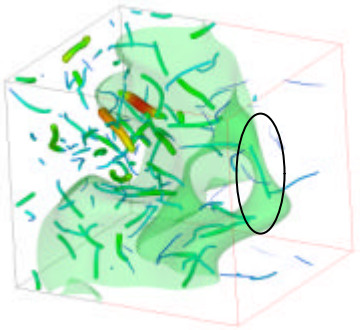

Fig. 7 Contour surface of temperature and axes of coherent fine scale eddy in corrugated flamelets.

Even though the heat release rate is highly fluctuating, its distribution shows three-dimensionally connected sheet-like structure (Tanahashi *et al.* 2002). For all cases, heat release rate tends to increase at the flame convex toward burned side. Figure 4 shows the distributions of mass fraction of O atom on a typical plane. The mass fraction of O atom tends to increase behind the flame front with high heat release rate for all cases. Miyauchi *et al.* (1997) has clarified the mechanism of increase of heat release rate and O atom. It is suggested that heat release rate increase is attributed to the same mechanism for all cases.

The distributions of the heat release rate in H_2-Case 2 at three different times are shown in Fig. 5. The unburned mixture appears behind flame front and seems to be isolated in the burned gas from the cross sectional viewpoint. The maximum heat release rate in the unburned mixture is 1.2 times of that of laminar flame and decreases rapidly down to 0.3 times of laminar flame at $0.2t_l$. Figure 6 shows the distributions of heat release rate for H_2-Case 1 at two different times. While turbulent premixed flames of H_2-Case 1 is classified in wrinkled flamelets, the unburned mixture is formed behind flame front with high heat release rate. Chen *et al.* (1998) have been conducted two-dimensional DNS of methane/air premixed flames and shown the presence of the pocket of unburned gas even in low turbulence intensity. To investigate the three-dimensional structure of unburned mixture, identification of axis of fine scale eddy is conducted (Tanahashi *et al.* 1999). Figure 7 shows the contour surface of temperature (=1400K) and axes of fine scale eddy around the unburned mixture for H_2-Case 2. As shown by the circle, the unburned mixture shows the three-dimensional structure like a handgrip and the region with high heat release rate is connected three-dimensionally. In the handgrip structure, the axis of fine scale eddy is perpendicular to the direction of mean flame propagation, which indicates that the handgrip structure is produced by the intrusion of the perpendicular eddy into the flame. The eddy transports the unburned mixture into the burned side and high heat release rate region is generated around the eddy. Three-dimensional structure like handgrip is one of the important structures that enhance the local heat release rate.

Figure 8 shows the distributions of vorticity, heat release rate, temperature and density for CH_4-air turbulent premixed flames (CH_4-Case 2). In distribution of vorticity, solid line is positive value and

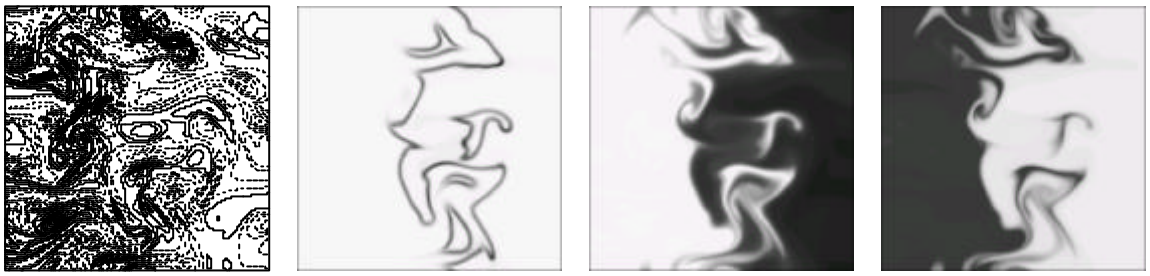

(a) vorticity (b) heat release rate (c) temperature (d) density

Fig. 8 Distributions of vorticity, heat release rate, temperature and density for CH_4-Case 2.

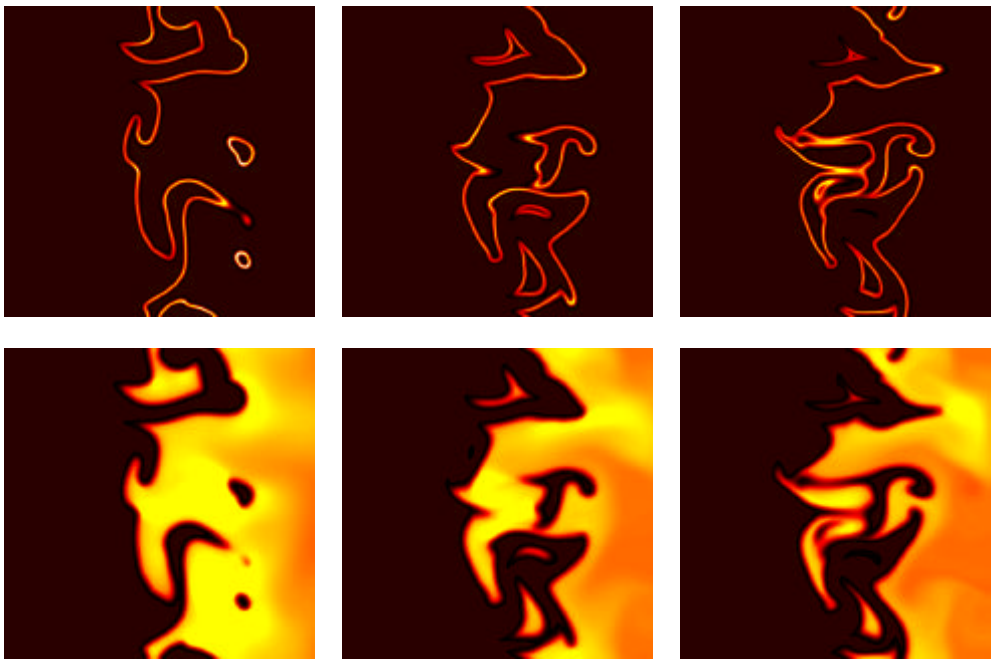

(a) CH_4-Case 1 (b) CH_4-Case 2 (c) CH_4-Case 3

Fig. 9 Distributions of the mole fraction of CH (upper) and OH (lower) for CH_4-Case 1 to CH_4-Case 3.

dashed line is negative. Vortices in the unburned side decay rapidly passing through the flame by the viscosity increase due to high temperature. Several vortices survive behind the flame front and the large modification of distributions of heat release rate, temperature and density due to turbulent motion can be observed. The vortex, which survives in the burned side, transports unburned mixture into the burned side and some vortices generates the pocket of unburned mixture. This result is similar to that reported by Chen *et al*. (1998). Furthermore, the vortex wrinkles the flame front largely and generates the pocket of burned gas in unburned mixture. At the cups of large wrinkled flames, it is observed that heat release rate is decreased rapidly, which is due to large strain rate tangential to flame front (Tanahashi *et al*. 2000).

The distribution of CH and OH mole fraction for CH_4-Case 1 to CH_4-Case 3 are shown in Fig. 9. The CH mole fraction is also modified by the turbulent motion. The thickness of CH mole fraction is thin and the distribution of CH mole fraction agrees with that of heat release rate. Moreover, the distribution of CH mole fraction can represent the pocket of unburned mixture and burned gas. Though the fluctuation of CH mole fraction and heat release rate become larger with increase of turbulence intensity, these distribution agree with each other. These results indicate that distribution of heat release rate can be predicted by that of CH mole fraction regardless of turbulent characteristics. OH mole fraction shows the high value in burned side. From distributions of OH mole fraction, the pocket can be observed.

3. CH/OH planar laser-induced fluorescence measurements in turbulent premixed flames

3.1 CH/CH planar laser-induced fluorescence

The schematic diagram of the experimental setup for simultaneous CH and OH PLIF measurement is shown in Fig. 10. For CH-PLIF measurement, the $Q_1(7,5)$ transition of the $B^2\Sigma^- - X^2\Pi(0,0)$ band at 390.30nm was excited and fluorescence from the A-X(1,1), (0,0) and B-X(0,1) bands between 420 and 440nm was detected (Garland *et al.* 1985, Carter *et al.* 1998). Many groups have conducted successful CH PLIF measurements using this transition (Han *et al*. 2000, Watson *et al.* 2000). The laser system consists of a XeCl excimer laser (Lambda Phisik, LPX 110I, 308nm, 200mJ/pulse) and a dye laser

(Lambda Phisik, Scanmate 2), and generates laser pulses with about 23-25mJ/pulse. The XeCl excimer pumped dye laser system with BiBuQ dye in p-Dioxane solvent, of which pulse width is 10-20ns. The collection optics was located perpendicular to the laser sheet. An intensified CCD camera (Andor Technology, DH734-25U-03) with 105mm F4.5 UV lens was used for the imaging. In order to block the flame radiation, 3mm thick interference filter (KV-418 Scott) was used. To optimize signal-to-noise ratio, all measurements were conducted with an image intensifier gate time of 30ns; this value was determined by preliminary experiments with a different gate time.

For OH PLIF measurement, the laser system consists of an Nd-YAG laser (Spectra-Physics, Quanta Ray PRO-110, 532nm, 350mJ/pulse) and a dye laser (Sirah Precisionscan), and generates laser pulses about 5mJ/pulse. The Nd-YAG laser pumped dye laser system at 282.93nm with Rhodamine 590 dye in methanol solvent, of which pulse width is 8-12 ns. The fluorescence from the A-X(1,0) and (0,0) bands (λ=306-320nm) was collected with a UV-Nikkor 105mm/f4.5 lens and imaged onto a second intensified CCD camera (PI-MAX, 512RB-G1). This camera, which is located on the opposite side of the burner from the intensified CCD camera for CH, was fitted with WG305 and UG-11 interference filters to reject incident light. Temporal separation of the CH and OH probe lasers was set to within 20ns. For PLIF, the laser beam is shaped into a thin (200μm) vertical sheet 10-mm high to optimize the signal to noise ratio. The PLIF system.affords a field of view of 27.6-mm × 27.6-mm at a resolution of 0.027-mm/pixels for CH and 0.054-mm/pixels for OH. From the averaged laminar flame images of slot flame burner, the laser beam intensity in the vertical direction was corrected.

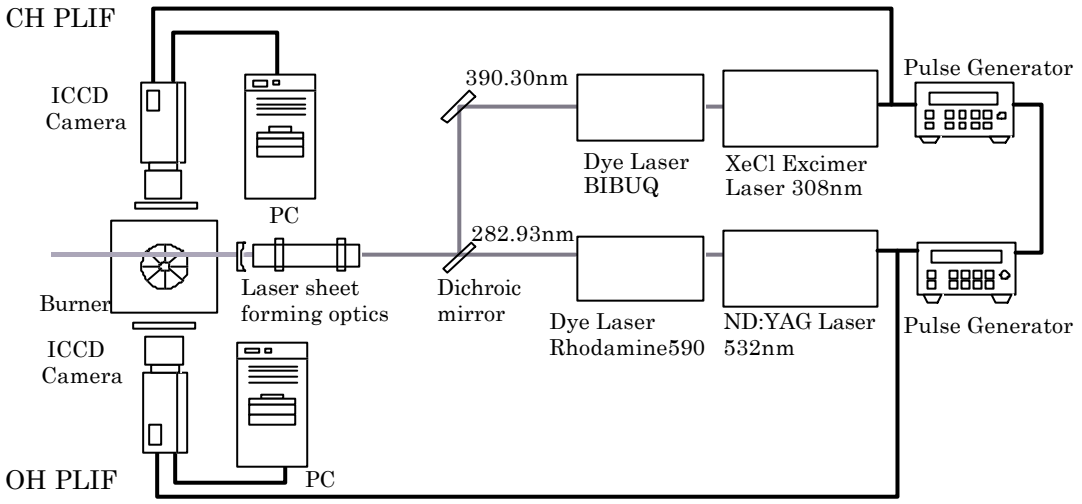

Fig. 10 The laser system for CH-OH planar laser-induced fluorescence measurements.

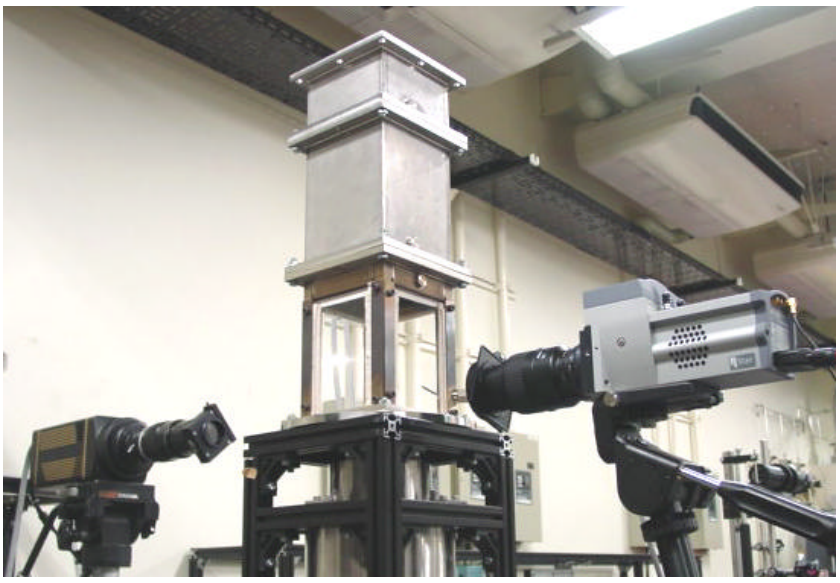

(a) Overview of the swirl burner.

(b) Swirl nozzle

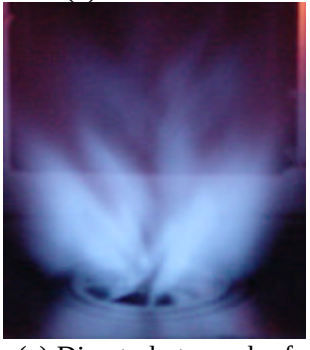

(c) Direct photograph of flame

Fig. 11 The laboratory swirl burner.

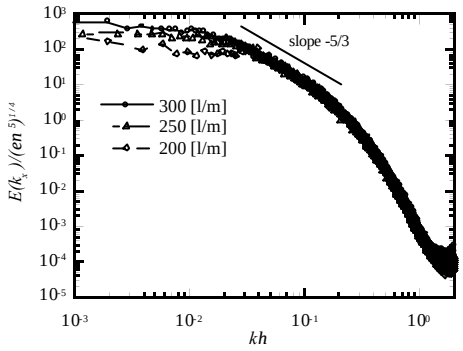

Fig. 12 Energy spectrum in the streamwise velocity.

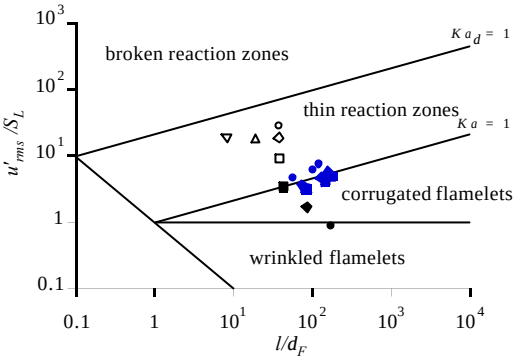

Fig. 13 Experimental conditions in turbulent combustion diagram.

Table 2 Experimental parameter and turbulence characteristics.

	f	Q [l/min]	Re_l	Re_λ	l/d_F	u'_{rms}/S_L	l (mm)	λ (mm)
E-CH_4-Case 1	1.1	200	265.8	63.1	82.3	3.23	3.42	0.812
E-CH_4-Case 2	1.1	250	602.0	95.0	145.0	4.15	6.02	0.950
E-CH_4-Case 3	1.1	300	881.0	115.0	175.3	5.03	7.27	0.949
E-CH_4-Case 4	1.0	200	265.8	63.1	82.9	3.20	3.42	0.812
E-CH_4-Case 5	1.0	250	602.0	95.0	146.0	4.12	6.02	0.950
E-CH_4-Case 6	1.0	300	881.0	115.0	176.6	4.99	7.27	0.949
E-CH_4-Case 7	0.9	200	265.8	63.1	73.6	3.61	3.42	0.812
E-CH_4-Case 8	0.9	250	602.0	95.0	129.7	4.64	6.02	0.950
E-CH_4-Case 9	0.9	300	881.0	115.0	156.8	5.62	7.27	0.949
E-CH_4-Case 10	0.8	200	265.8	63.1	57.1	4.65	3.42	0.812
E-CH_4-Case 11	0.8	250	602.0	95.0	100.6	5.98	6.02	0.950
E-CH_4-Case 12	0.8	300	881.0	115.0	121.6	7.24	7.27	0.949

3.2 Effects of Rynolds number and equivalent ratio on the flame structure

Figure 11 shows the overview of the swirl burner, swirl nozzle and formed flame at stoichiometric condition of 300 [l/min] flow rate. This combustion rig consists of a rectifying section, a swirl nozzle section and combustion chamber including contraction part angled 45 deg. The inner diameter of 120-mm in the rectifying section is contracted to 40-mm diameter. The swirl nozzle of 40-mm inner diameter was mounted on the rectifying section.

The inner cross-section of combustion chamber was 120-mm × 120-mm, and the length of the chamber was 550-mm. On every side of combustion chamber, a silica glass plate of 120-mm × 170-mm and 5-mm thickness was installed to allow optical access. The outlet of combustion chamber was contracted to 60-mm × 60-mm. The total length of combustion chamber was 590-mm. The swirl nozzle has swirl vanes of 14-mm inner diameter and 40-mm outer diameter, angled 45 deg from the nozzle axis. Though secondary nozzle exit was mounted at center of the swirl vanes, this secondary one was not used in present study. The premixed air and methane pass through the swirl vanes and the flame was stabilized at swirl vanes as shown in Fig. 11(c).

We examined 3 kinds mixture flow rate and 4 kinds of equivalence ratio as shown in Table 2. The flow rates, Q, and equivalence ratio, f, vary from 200 to 300 [l/min] and from 0.8 to 1.1, respectively. To investigate the turbulent characteristics of unburned mixture, two component of velocity were measured across 13-mm downstream of swirl nozzle exit by using a hot-wire. CH/OH PLIF measurements were conducted at maximum u'_{rms} cross-section, where u'_{rms} indicates r.m.s value of velocity fluctuations.
Figure 12 shows the energy spectrum in the streamwise velocity of maximum u'_{rms} regions. For every conditions, the energy spectrum shows –5/3 power law and it demonstrates that the flow field, where CH/OH PLIF measurement was conducted, was fully developed turbulence. The turbulence characteristics estimated by velocity fluctuations were shown in Table 2, where l is integral length scale, Re_l is Reynolds number based on integral length scale, Re_λ is Reynolds number based on Taylor micro scale, d_F is laminar flame thickness and S_L is laminar burning velocity.

Based on turbulence and flame characteristics as shown in Table 2, each experimental condition has been appeared in the turbulent combustion diagram as shown in Fig. 13 (blue color). For every flow rate conditions, the combustion regime of experimental conditions positioned at boundary layer between corrugated flamelets and thin reaction zones. In addition, the combustion regime was shifted from

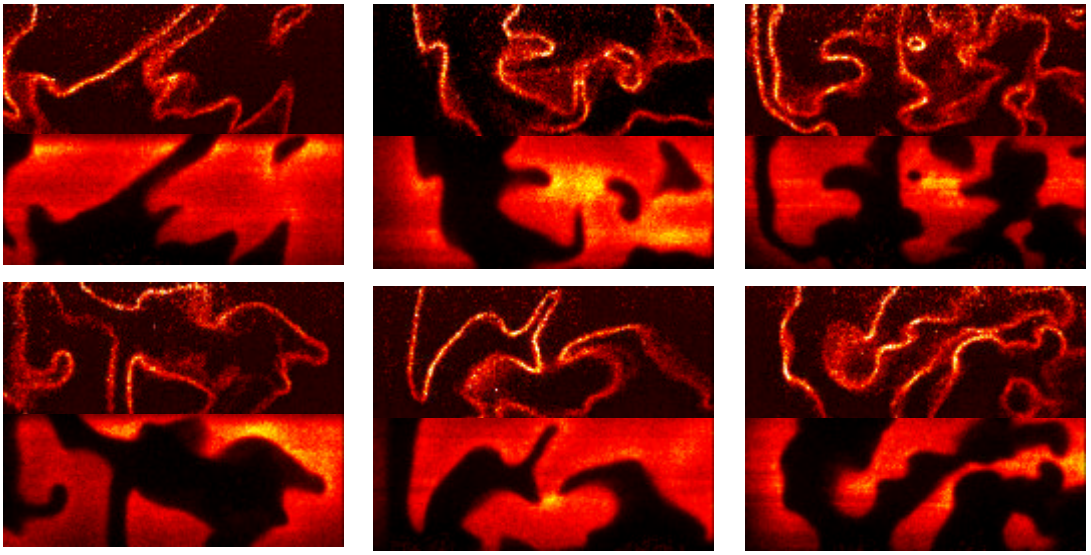

(a) Q=200[l/min] (Re_l=63.1) (b) Q=250[l/min] (Re_l=95.0) (c) Q=300[l/min] (Re_l=115.0)

Fig. 14 CH fluorescence images (upper) and OH fluorescence images (lower) in CH4-air turbulent premixed flames with different Reynolds number on the swirl burner.

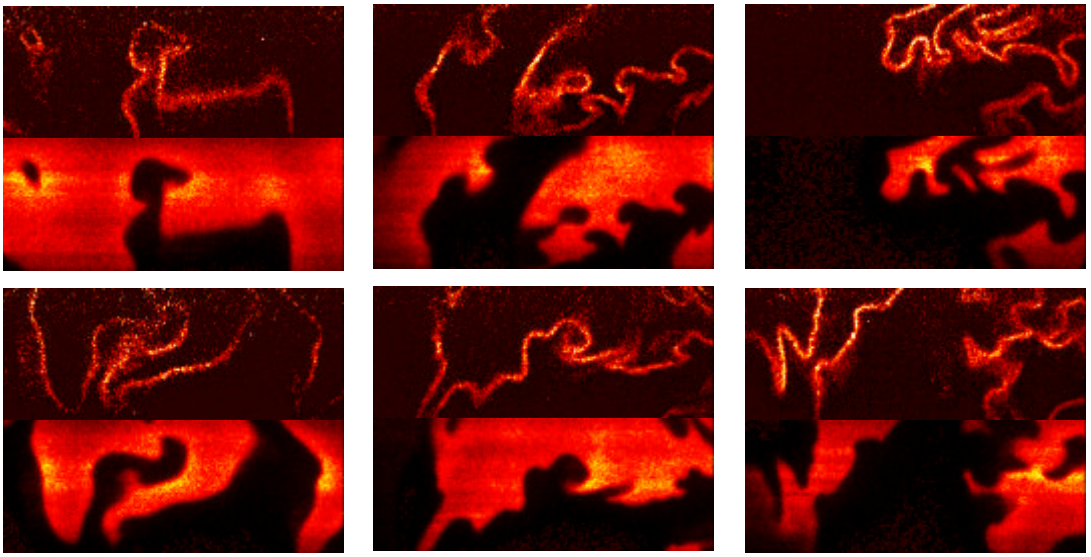

(a) f=0.8 (b) f =0.9 (c) f =1.0

Fig. 15 CH fluorescence images (upper) and OH fluorescence images (lower) in CH_4-air turbulent premixed flames with different equivalent ratio on the swirl burner (Q=300[l/min], Re_l=115.0).

corrugated flamelets to thin reaction zones with decreasing equivalence ratio. For f = 0.8, every flow rate conditions positioned at thin reaction zones. From combustion diagram, it is expected that the local flame structure becomes complicated with decreasing equivalence ratio.

3.3 Local flame structures obtained by CH/OH PLIF

To compare the local flame structure as a function of Reynolds number, three sets of CH and OH PLIF images (25-mm (W) × 9.7-mm (H)) were shown in Fig. 14. Each Reynolds number condition shows two different images. The products region appears bright. CH images represent the distribution of a very short-life combustion intermediate that can be interpreted as the primary flame front. On the other hand, OH fluorescence shows high intensity in the fuel-lean region and is mostly present in hot combustion products. Thus, the simultaneous measurement of CH and OH show the boundary of the hot products with the cold reactants. These images clearly demonstrate flame wrinkling. The images may be interpreted as the instance during which the flames interact with turbulence scales such as integral length scale and Taylor micro scale. For every Reynolds number condition, flame wrinkling and flame front cusps was observed, and the scale of weak wrinkled flame and flame cusps corresponds to integral length scale and Taylor micro scale, respectively. We can observe that local flame structure becomes more complicated and the frequency of flame cusps, corresponding to order of Taylor micro scale, became higher

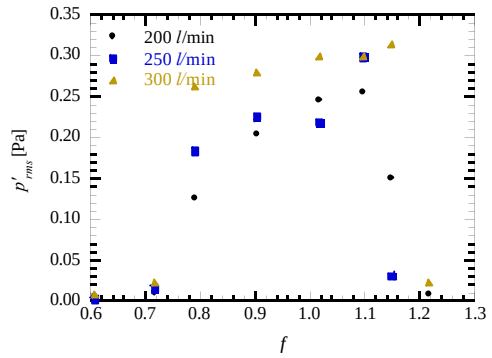

Fig. 16 Variations of the intensity of pressure fluctuations.

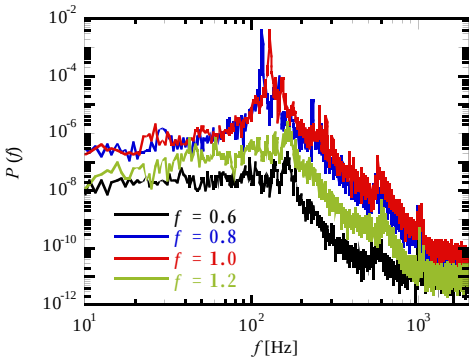

Fig. 17 Power spectrum of the pressure fluctuations.

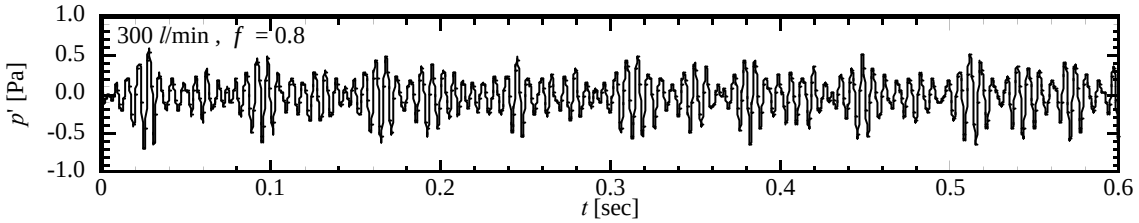

Fig. 18 Time-series signal of pressure fluctuations.

with increasing Reynolds number. The complicated flame structure is ascribed to increased turbulence intensity of unburned mixture.

Figure 15 shows CH/OH PLIF images as a function of equivalence ratio at Re_l = 115, Q = 300 [l/min]. Although the scale of weak wrinkled flame keeps the same order of the integral length scale in terms of equivalence ratio, the frequency of flame front cusps became higher with increasing equivalence ratio. Considering flame regime on the turbulent combustion diagram, it is quite curious result. Because the turbulence characteristics of unburned mixture might be influenced by combustion-induced pressure oscillation, additional investigation of turbulence characteristics in reacting condition is necessary to provide detail information about local flame structure in the turbulent premixed flames.

3.4 Pressure fluctuation in the swirl burner

To investigate the influence of combustion-induced oscillation on local flame structure, simultaneous measurement of CH/OH PLIF and pressure fluctuation was achieved. The pressure transducer (Toyoda, PD104) was used for measuring pressure fluctuations in the combustion chamber. The maximum response frequency of the pressure transducer was 1kHz. A water-cooled connecting tube was used to connect the pressure transducer and combustion chamber. The signal from the pressure transducer was amplified by a DC amplifier (Toyoda, AA6210) and stored in the PC through the A/D converter (NEC Loggerstation DL2300AP). Pressure fluctuations were measured at the position 245-mm downstream of the swirl nozzle exit. Figure 16 shows variations of the intensity of pressure fluctuations with the supplied flow rates and equivalence ratio. In addition, the power spectrum of the pressure fluctuations at Q = 300 [l/min] was also shown in Fig .17. Regardless of Reynolds number, the r.m.s. value of pressure fluctuations shows large values between f = 0.8 and 1.1. For the large pressure fluctuation region, the frequency corresponding to the highest peak lay between 117Hz and 130Hz. Because the flame stabilized on the tip of swirl vanes for these large pressure conditions, we focused on these conditions to investigate the local flame structure near flame holder. Figure 18 shows the time-series signal of pressure fluctuations at 300 [l/min], f = 0.8. Periodic signals were observed with two components of 30Hz (long period) and 117Hz (short period).

To investigate the relation between relatively long period of pressure and local flame structure, we classified into three large groups, that is, small pressure fluctuating region (A), middle pressure fluctuating region (B) and large pressure fluctuating region (C) in the long period of pressure fluctuations, as shown schematically in Fig. 19.

Figure 19 shows CH/OH PLIF images (25-mm (W) × 9.7-mm (H)) classified into large three groups. For the small pressure fluctuating region (A), the flame front is very smooth and has only slight wrinkling. The formation of flame cusps is also rare compared to other conditions. The scale of weak wrinkled flame

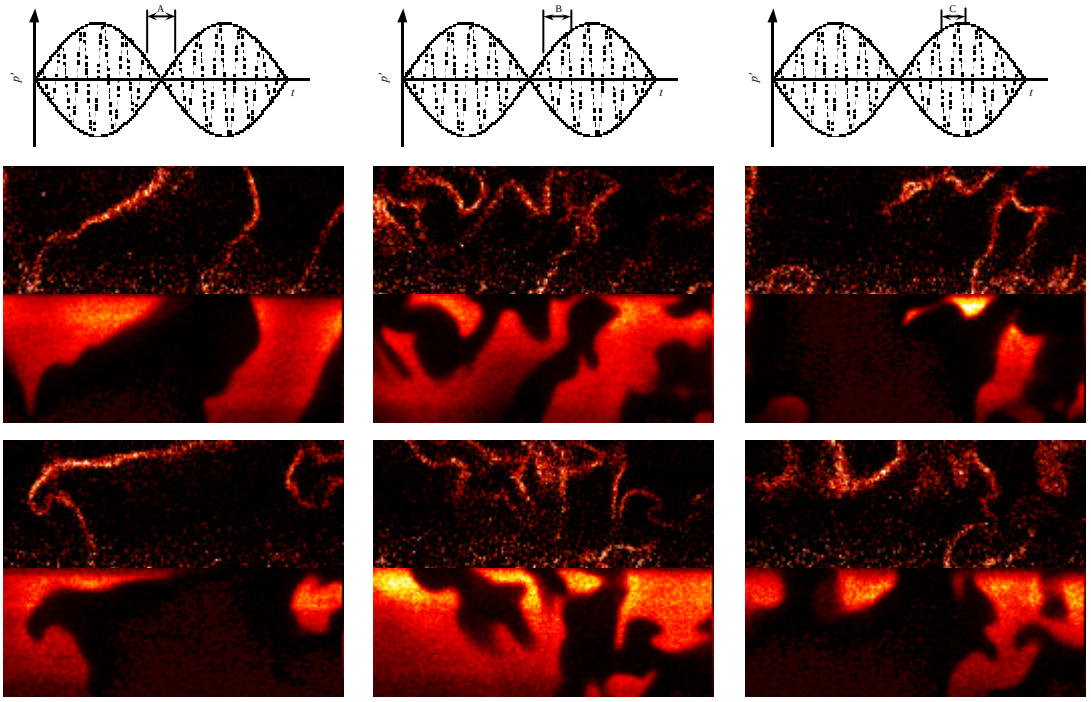

(a) A region (b) B region (c) C region

Fig. 20 CH fluorescence images (upper) and OH fluorescence images (lower) in CH4-air turbulent premixed flames with different Reynolds number on the swirl burner (Q=300[l/min], Re_l=115.0, f=0.8).

front corresponds to the integral length scale of unburned mixture. For the middle pressure fluctuating region (B), the degree of flame wrinkling and features was changed compared to A region. The flame is much more wrinkled and many small-scale flame cusps were observed. The scale of cusps corresponds to the order of Taylor micro scale. For the large pressure fluctuating region (C), we can observe that small-scale flame cusps remained though flame front became rare compared to B region. The local flame structure is influenced by pressure fluctuations. These results demonstrate a relation between long period of pressure fluctuations and local flame structure. Additional investigation, however, is necessary to clarify the mechanism in detail.

4. Summary

In this study, three-dimensional DNS of H_2-air premixed flames and two-dimensional DNS of CH_4-air turbulent premixed flames have been performed to investigate the local flame structure in turbulent premixed flames. From DNS of H_2-air premixed flames, it is clarified that the local flame structure of wrinkled flamelets is also modified by the turbulence motion and heat release rate tends to increase at the flame convex toward burned side regardless of turbulent characteristics. Three-dimensional handgrip structure is observed behind the flame front. This structure is generated by fine scale eddy. The unburned mixture in handgrip structure is burned rapidly, which lead to increase heat release rate compared with that of laminar flame. For two-dimensional DNS of CH_4-air turbulent premixed flames, a pocket is observed in both unburned and burned side. It is clarified that the distribution of heat release rate agrees with that of CH mole fraction even in high intensity turbulent premixed flames. This result shows the availability of CH radical as a marker for heat release rate.

The local flame structure and pressure fluctuations in the oscillating turbulent premixed flame are investigated by CH/OH PLIF and pressure measurement. From the simultaneous measurement of CH/OH PLIF, it is shown that the degree of wrinkling changed in terms of Reynolds number and equivalence ratio, and the local flame structure became more complicated with increasing Reynolds number. The observed scale of weak wrinkled flame front and flame cusps corresponds to integral length scale and Taylor micro scale, respectively. The local flame structure is influenced by pressure fluctuations in the oscillation turbulent flames, and a relation between local flame structure and long period of pressure fluctuation is observed.

References

Allen, M., Howe, R. D. and Hanson, R. K. (1986), Opt Lett. 11:126-128.

Baum, M., Poinsot, T., Haworth, D. and Darabiha, N. (1994), J. Fluid Mech. 281: 1-32.

Baum, M., Poinsot, T. and Thevenin, D. (1994), J. Comput. Phys. 116: 247-261.

Carter, C. D., Donbar, J. M. and Driscoll, J. F. (1998), Appl. Phys. B, 66: 129-132.
Chen, J. H., Echekki, T. and Kollmann, W. (1998), Combust. Flame 116: 15-48.
Comte-Bellot, G. and Corrsin, S. (1971), J. Fluid Mech. 48: 273-337.
Garland, N.L., and Crosley, D. R. (1985), Appl. Optics 24: 4229-4237.
Gutheil, E., Balakrishnan, G. and Williams, F. A. (1993), Reduced Kinetic Mechanisms for Applications in Combustion Systems, Peters, N. and Rogg, B. ed., Springer-Verlag: 177-195.
Han, D., and Mungal, M.G. (2000), Proc. Combust. Inst. 28: 261-267.
Harper, J., Johnson, C., Neumeier, Y., Lieuwen, T., and Zinn, B. T. (2001), AIAA Paper-01-0486.
Haworth, D., Blint, R., Poinsot, T. and Cuenot, B. (2000), Combust. Flame 121: 395-417.
Kee, R. J., Dixon-Lewis, G., Warnatz, J., Coltrin, M. E. and Miller, J. A. (1986), Sandia Report, SAND86-8246.
Kee, R. J., Rupley, F. M. and Miller, J. A. (1989), Sandia Report, SAND89-8009B
Lee, J. G., Kim K., and Santavicca, D. A. (2000), Proc. Combust. Inst. 28: 739-746.
Mansour, M. S., Peters, N. and Chen, Y.-C. (1998), Proc. Combust. Inst. 27: 676-773.
Miyauchi, T., Tanahashi, M., Sasaki, K., and Ozeki, T. (1996), Transport Phenomena in combustion, Chen, C. H. ed., Taylor & Francis, New York: 1095-1105.
Miyauchi, T., Tanahashi, M., Imamura, Y. and Nada, Y. (1997), Proc. 1st ASPACC: 278-281.
Paschereit, C. O., Gutmark, E., and Weisenstein, W. (1999), Physics Fluids, 11-9: 2667-2678.
Peters, N. (2000), Turbulent Combustion, Cambridge univ. press.
Poinsot, T. J. and Lele, S. K. (1992), J. Comput. Phys. 101: 104-129.
Putnum, A.A. (1971), Combustion-Driven Oscillations in Industry, Elsevier, London
Tanahashi, M., Miyauchi, T. and Ikeda, J. (1997), Proc. 11th Symp. Turbulent Shear Flow 1: 4-17-4-22.
Tanahashi, M., Iwase, S., Uddin, M. A. and Miyauchi, T. (1999), Turbulence and Shear Flow Phenomena – 1, Banaerjee, S. and Eaton, J. K. ed., Begell House Inc.: 79-84.
Tanahashi, M., Miyauchi, T., Saito, T. and Shimamura, M. (1999), Proc. 2nd ASPCC: 500-503.
Tanahashi, M., Fujimura, M. and Miyauchi, T. (2000), Proc. Combust. Inst 28: 529-535.
Tanahashi, M., Saito, T. and Miyauchi, T. (2000), Proc. 4th JSME-KSME Thermal Engineering Conf. 3: 97-102.
Tanahashi, M., Ito, Y., Yu, Y. and Miyauchi, T. (2001), Proc. 3rd ASPCC: 75-78.
Tanahashi, M., Nada, Y., Ito, Y. and Miyauchi, T. (2002), Proc. Combust. Inst. 29, in press.
Watson, K.A., Lyons, K. M., Donbar, J.M., and Carter, C.D. (2000), Combust. Flame 123: 252-265.